Environ Biol Fish (2013) 96:1045–1063
DOI 10.1007/s10641-012-0102-6

Effects of prey size structure and turbulence on feeding and growth of anchovy larvae

Agurtzane Urtizberea · Øyvind Fiksen

Received: 6 October 2011 / Accepted: 14 December 2012 / Published online: 30 January 2013

Abstract Foraging processes in plankton and planktivorous fish are constrained by relative prey and predator size and therefore, these are important variables to include in a foraging model. The distribution of prey biomass across different size classes can be characterized by a size spectrum slope. We present a foraging model for anchovy larvae including the most relevant processes such as prey encounter, capture- and pursuit success, all influenced by light, turbulence and prey characteristics. We modelled ingestion rates and specific growth rate by coupling the foraging model with an existing bioenergetic model, and performed a sensitivity analysis of prey ingestion in turbulent environments assuming either hemispherical or conical perceptive volume. Our results suggest that turbulence has no positive effect because of the low capture ability, small prey size and small visual volume for anchovy larvae. The predicted ingestion is too low to sustain the growth potential of larvae when assuming conical perceptive volume even under prey densities substantially higher than normally found in the field. Ingestion rate is sensitive to the total biomass and the slope of the prey size spectra, specifically because it determines the abundance of prey around the optimal size for the larvae. The model also suggests that small larvae benefit from a prey size structure with steep prey size-spectra slope while a large larva benefit from less steep slopes. The model can act as a link between size-spectra measurements from the field and the foraging conditions of larval anchovies.

Keywords Fish larva · Prey size spectra · Foraging model · Turbulence · Visual perceptive volume

Electronic supplementary material The online version of this article (doi:10.1007/s10641-012-0102-6) contains supplementary material, which is available to authorized users.

A. Urtizberea · Ø. Fiksen
Department of Biology, University of Bergen,
P.O.Box 7803, 5020 Bergen, Norway

Ø. Fiksen (✉)
Uni Research,
P.O. Box 7810, 5020 Bergen, Norway
e-mail: Oyvind.Fiksen@bio.uib.no

Present Address:
A. Urtizberea
Marine Research Dvision, Azti Foundation,
Txatxarramendi ugartea 8 z/g,
48395, Sukarrieta, Bizkaia, Spain

Introduction

Many studies have assessed larval survival and growth with biophysical models coupling physical transport and larval fish growth models (Werner et al. 1996; Heath and Gallego 1998; Rose et al. 1999; Hermann et al. 2001; Hinckley et al. 2001; Hinrichsen et al. 2002; Kristiansen et al. 2007; Vikebø et al. 2010). Some models assimilate prey fields from direct estimations of field data based on specific species or stage of potential prey (Hinrichsen et al. 2002; Lough et al. 2005; Kristiansen et al. 2009a). Other models introduce mean prey densities obtained from marine ecosystem models (Hermann et al. 2001; Hinckley et al. 2001; Daewel et al. 2008b) or from individual based models (IBMs) of prey (Kristiansen et al. 2008,

2009b). Daewel et al. (2008a) developed a new approach to estimate size structured prey fields from bulk zooplankton estimates in a NPZ-model. Kühn et al. (2008) coupled a biophysical model and an IBM of larval fish in order to identify potential areas that support larval survival and growth in time and space, using a stage specific prey field transformed into prey size distributions. Here, we explore the impact of prey abundance on ingestion rates with theoretical size spectra, a format resembling how data from the field often are presented.

Sheldon et al. (1977) defined biomass size spectra as the biomass distribution over a sequence of logarithmically fixed body size intervals. A size spectrum describes the size-structure of a pelagic community and allows one to compare communities using estimates of slopes and intercepts. In addition, statistical analysis of biomass size spectra also shows the efficiency of energy transfer between trophic levels in a community. The recent innovations in image analysis (Grosjean et al. 2004; Davis et al. 2005; See et al. 2005) enable fast estimates of biomass size spectra in the field (Ashjian et al. 2001; San Martin et al. 2006; Zarauz et al. 2007; Irigoien et al. 2009). The simplicity of the size spectra facilitates their inclusion into foraging models to understand how feeding behaviour, survival and growth of larvae in the field depend on successful surfing on size-spectra (Pope et al. 1994), growing as fast as the prey with the highest density.

We focus on the early life stage, when larvae switch from subsisting on their endogenous yolk sac to first feeding, often referred to as a critical phase in larval fish ecology. During this stage the larvae have high mortality rates and a high growth rate is essential to their survival. Foraging models of fish larvae have focused mainly on larval length, prey density, light and turbulence (Werner et al. 1996; Fiksen et al. 1998; Letcher et al. 1996; Fiksen and Folkvord 1999; Hinrichsen et al. 2002; Lough et al. 2005). The prey encounter rate is very sensitive to the visual abilities of fish larvae (Fiksen et al. 1998). Models show that turbulence enhances the encounter rate between larvae and prey (Rothschild and Osborn 1988; Matsushita 1992) depending on the shape of the perceptive volume (Galbraith et al. 2004; Lewis and Bala 2006; Mann et al. 2006; Mariani et al. 2007). On the other hand, what is customary termed 'pursuit success' (the probability that prey is not advected away before a strike position is reached) is shown to decrease with turbulence (MacKenzie et al. 1994; MacKenzie and Kiørboe 2000). Typically, models of prey encounter rates in larval fish assume a spherical or hemispherical perceptive volume, but laboratory observations suggest that the visual perceptive volume, for example in anchovy larvae, may be cone-shaped (Hunter 1972; Chesney 2008). After coupling the encounter rate and the pursuit success, theory and experimental evidence suggests that ingestion rate peak at intermediate turbulence levels (MacKenzie et al. 1994; MacKenzie and Kiørboe 2000).

We chose anchovy larva *Engraulis mordax* as our model species. Anchovy is important in linking lower and higher trophic level in many upwelling ecosystems (Cury et al. 2000). In addition, there exist comprehensive laboratory experiments studying the feeding behaviour of anchovy larvae (Hunter 1972, 1977) which serve as valuable guides during the development of a foraging model. We developed a foraging model for anchovy larvae and combine this with theoretical prey size distributions estimated from normalized biomass size spectra (NB-S spectra), and explore how different prey size structures influence feeding success of anchovy larvae. In addition, the foraging model is coupled to a bioenergetic model developed for anchovy larvae in an earlier study (Urtizberea et al. 2008). Our objectives are to model larval ingestion and growth rates under variable environmental conditions and analyze how size spectra can be applied as prey fields. This is needed in several contexts, such as biophysical modelling of environmental effects on recruitment success or in models to better understand behaviour and trade-offs in larval fish.

Methods

Model description

The model description follows the outline recommended by Grimm et al. (2006, 2010) for presentation of individual based models (IBMs). The computer code (FORTRAN) is available on request.

Purpose

We developed a model to represent the feeding process of an anchovy larva under different biotic and

abiotic conditions; including prey size spectra, turbidity, turbulence and in order to calculate growth, we coupled it with a bioenergetic model previously developed by Urtizberea et al. (2008) for anchovy larvae (Fig. 1). The model predicts ingestion rates per second, as a consequence of prey encounter rates and capture success. Growth depends on dynamic gut content and temperature, and is integrated with hourly time steps (Fig. 1). The aim of our study is to create a foraging model for fish larvae between 4 and 8 mm using a similar prey size structure descriptor as in field studies. The capture success model was parameterized from literature data for larvae until 11 mm. However, the bioenergetic model was parameterized with data of larvae until 8 mm only, so the complete model is valid for larvae from 4 to 8 mm. We also investigate the effects of prey size distributions and environmental variables on the feeding success.

Foraging processes

A sequence of events is necessary for successful ingestion of prey in a planktivorous fish (Fig. 1). First an encounter between prey and larva must take place. Then the larva may try to capture the prey, which requires successful pursuit and approach of prey. The separation of these two events is artificial, but practical; since the prey must remain within sight for the time it takes to pursue the prey (MacKenzie et al. 1994) and it needs to approach the prey to a distance where it can strike and ingest it without being detected (Kiørboe and Visser 1999). The pursuit depends on the turbulence level (MacKenzie and Kiørboe 2000) and the visual perception distance of the larva (Fiksen and MacKenzie 2002). Furthermore, a successful capture also depends on what we call the larval capture ability, the precision of the final larval strike to capture the prey (Hunter 1972) and the relative size of the prey item. If all events are successful then the larva ingests the prey. Here we assume larvae approach to a fixed distance from the prey, i.e. we only consider two probabilities, pursuit *Pps* and the capture ability *P*ca.

There are no available studies describing the feeding behaviour of *E. mordax* anchovy larvae in the field, however, many studies show that European anchovy larvae can feed on a range of different prey sizes (García and Palomera 1996; Conway et al. 1998; Tudela et al. 2002; Catalán et al. 2010; Morote et al. 2010). Therefore ingestion, I ($\mu g s^{-1}$), is calculated from the Holling disk equation for multiple prey

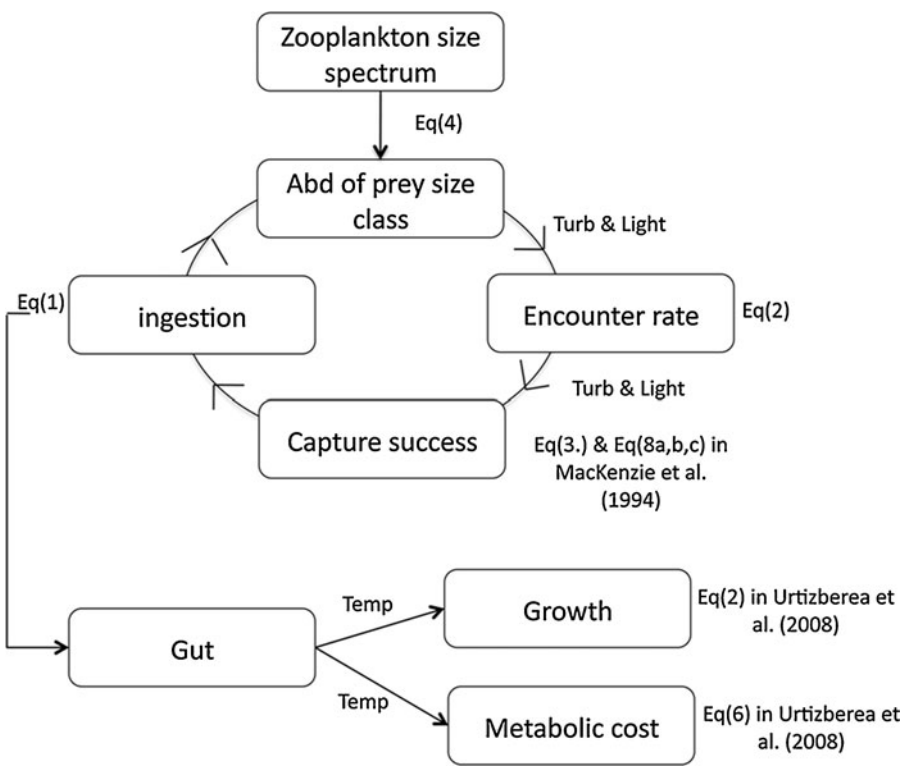

Fig. 1 Flowchart represents the modelled processes in order to simulate the feeding process and growth of an anchovy larva in 1 h. Encounter rate and capture success depend on turbulence and light, while growth and metabolic cost on temperature. Capture success is a combination of larval ability [Eq. (3.5) and pursuit success (1994)]. Bioenergetic model was previously developed by Urtizberea et al. (2008)

(Stephens and Krebs 1986; Holling 1966):

$$I_j = \frac{\sum_i e_{i,j} Pcs_{i,j} wp_i}{1 + \sum_i e_{i,j} h}, \quad (1)$$

where j denotes a given size of larva and i a given size of prey, $e_{i,j}$ is the encounter rate (prey s^{-1}) (see below), $Pcs_{i,j}$ is the capture success (see Table 1), wp_i (μg dw) is the prey dry weight (see Eq. 4.4) and h is prey handling times, the total time required for the larvae to pursue, capture and consume the prey. The feeding sequence measured in laboratory experiments lasted from 1 to 2 s (Hunter 1972). There are no reports of handling time of different sizes of prey for anchovy larvae, so we use a fixed handling time for any size of prey, h=1.5 s. Here, we have not made any attempts to model the optimal diet breadth, see Visser and Fiksen (2012) for an algorithm of how this element of larval fish feeding could be added to the current model.

Encounter rate

Existing evidence suggest a positive effect of turbulence on the clearance rate (Sundby and Fossum 1990;

Table 1 Parameter's and variable's description, unit, value or source and reference

Symbol	Description	Unit	Value, source	Reference
j	Standard length of the larva	m	0.004 and 0.008	
i	Prey length	mm		
$e_{i,j}$	Encounter rate	Prey s^{-1}	Eq. (2)	
$Pcs_{i,j}$	Capture success	Dim.less	$Psp_{i,j} \times Pca_{i,j}$	
$Pps_{i,j}$	Pursuit success	Dim.less		(1)
$Pca_{i,j}$	Capture ability	Dim.less	Eq. (3.5)	
C_m	Numerical constant corrected depends on the shape of encounter regions	Dim.less	6×0.2–for a cone of 26º 6×0.8–for a semispherical shape (180º)	(7)
$r_{i,j}$	Perception distance	m		(4)
φ	The angle of visual perception of larvae	°	26 or 90	(2)
c	Beam coefficient	m^{-1}	0.3	
$A_{p,i}$	Area of prey image	m^2		
E'_j	Visual sensitivity of a larva	Dim.less	$E'_j = \frac{(0.82j)^2}{C \times 0.000133 \times 0.0002 \times 0.75}$	
C	Prey inherent contrast	Dim.less	0.3	(3)
E_b	Light at surface, midday	$\mu mol\, m^{-2} s^{-1}$	3000	
K_e	Light satiation of the predator	$\mu mol\, m^{-2} s^{-1}$	5	(4)
N_i	Prey density	Prey m^{-3}		
V_j	Larval velocity	$m\, s^{-1}$		(2)
dp_i	Width of prey	mm	Table A1, A2 and A3. see supplementary material	
lp_i	Length of prey	mm	Eq. (4.3)	(6)
wp_i	Weight of prey	μg	Eq. (4.4)	(5)
ε	Turbulent dissipation rate	$m^2 s^{-3}$	From 10^{-10} to 10^0	
h	Handling time	s $prey^{-1}$	1.5	(2)
B_i	Biomass in the size class i	$\mu g\, m^{-3}$	Table A1, A2 and A3, see supplementary material1.5	(2)
TB	Total biomass in all the prey size range	$\mu g\, m^{-3}$	20000	
a	Intercept of the normalized size spectra		Eq. 4.2	
b	Slope of the size spectra		0, −1, −2	

(1) (MacKenzie et al. 1994), (2) (Hunter 1972), (3) (Utne-Palm 1999), (4) (Aksnes and Utne 1997), (5) (Peters and Downing 1984), (6) (Conway et al. 1998), (7) (Pécseli and Trulsen 2007)

Muelbert et al. 1994; MacKenzie and Kiørboe 1995; Mann et al. 2005) and a negative effect on pursuit (MacKenzie et al. 1994; MacKenzie and Kiørboe 2000). The clearance rate is modeled as in Kiørboe and MacKenzie (1995), but it includes the dimensionless numerical constant correcting for conical perception volume with different opening angle, C_M (Pécseli and Trulsen 2007; Pécseli et al. 2010) (see Table 1):

$$e_{i,j} = \beta_{i,j} N_i = \sqrt{\left(C_M \varepsilon^{1/3} {r_{i,j}}^{7/3}\right)^2 + \left(\pi \left(r_{i,j} \sin \varphi\right)^2 V_j\right)^2} N_i. \quad (2)$$

Here $\beta_{i,j}$ is the clearance rate ($m^3 s^{-1}$), N_i is the abundance (prey m^{-3}), ε ($m^2 s^{-3}$) is the turbulent dissipation rate, $r_{i,j}$ (m) is the perception distance of a larva with size j on the prey size i and φ is the angle of the perception (Table 1). We assume prey motility is negligible and let V_j ($m s^{-1}$) represent the larval swimming velocity as a function of standard length j (Hunter 1972) (Table 1).

The model for visual detection distance, $r_{i,j}$ was developed by Aksnes and Giske (1993) and later modified by Aksnes and Utne (1997) and Fiksen et al. (1998). The model depends on ambient light E_b, beam attenuation c, area of prey image A_p prey inherent contrast C, the visual light sensitivity E'_j and the light satiation K_e of the predator (see Table 1). Parameterization of the eye sensitivity E'_j (Aksnes and Utne 1997; Fiksen and MacKenzie 2002) is made using the estimates of detection distance from laboratory experiments (Hunter 1972) and assuming that light was not a limiting factor in the laboratory experiment ($E_b >> K_e$) (Table 1):

$$E'_j(l) = \frac{{r_{l,j}}^2}{|C| A_p} \quad (2.1)$$

Here, A_p is the area of prey image and C is the inherent contrast of prey. To calculate the eye sensitivity it is necessary to know the size of prey A_p used by Hunter (1972). The prey in the experiment was *Brachionus*, *Artemia* nauplii, various veliger larvae and wild copepod larvae, but their size was not reported. To estimate eye sensitivity we use the mean length and width of a rotifer; 200 and 133 μm from Theilacker and McMaster (1971) and Hunter (1980), respectively. This prey size is consistent with the prey size range found in the gut of 5 day old anchovy larvae [75–150 μm; Theilacker (1987)].

Prey capture

We calculate ingestion rate as the product of prey encounter rate, capture ability and pursuit success (Table 1). The loss of prey due to turbulent velocity is termed 'pursuit success' while the loss due to prey escape is termed 'capture ability'.

Pursuit success

Pursuit success is calculated using the analytical model developed by Mackenzie et al. (1994), where they showed that larval pursuit success decreases with turbulence. They defined the probability of a successful pursuit as the probability that the prey remains in the encounter sphere during a minimum time frame t. The model assumes that the turbulence-generated velocity is constant within the perception sphere and that t is the minimum time required for a cruising larva to identify approach and attack the prey (handling time).

We assume that there is no difference in the pursuit success due to the shape in the assumed perceptive volume. A recent theoretical model (Pécseli et al. 2012), based on prey residence time in the perceptive volume, did show a more or less linear decrease in capture success with the opening angle of the cone. We have not included this in the current model, so the ingestion rates in cone-shaped visual spheres are likely lower than we predict here.

Capture ability

We use a mechanistic model of prey capture success calibrated with observational data from the literature. Even if the overall model only can be used to simulate larvae from 4 to 8 mm, the capture ability model is parameterized and calibrated for larvae from 4 to 11 mm (Hunter 1977). The capture success depends on the larval size, and larval cognitive and locomotory abilities (Hunter 1972), in addition to prey size and prey escape responses (Caparroy et al. 2000). Our model is a combination of the models developed by Beyer (1980) and Fiksen and Mackenzie (2002). The capture success is formulated in terms of predator mouth size, the precision in the feeding strike, strike distance, prey escape direction, and the relative

velocity of attack and escape in predator and prey. There is no learning effect in capture ability.

Beyer (1980) modeled the feeding strike as shots fired at a target, assuming that the target does not move, i.e. the prey has no escape response, with (x, y) representing the coordinates of the mouth center (bull's eye) relative to the prey center after the strike. Beyer did not include the strike distance between the larva and prey before the strike. This is needed to include the escape behaviour of the prey. Here, we assume attack occurs in two-dimensions with x=0 and y normally distributed with mean zero and σ^2 variance (Beyer 1980). When the prey has no escape response the distance between larva's mouth and the prey after the strike is $z = y$, and the larval strike angle before the strike is: $\alpha = arctan(z/r_s)$, where r_s is the strike distance (Fig. 2, Table 2). The larva captures the prey if the prey center point is inside the mouth area, that is if

$$z \leq (m - dp)/2, \tag{3.1}$$

where m is the larval mouth size (Table 2) and d_p is the prey width.

The precision parameter, σ=0.06 mm was estimated by Beyer (1980), assuming that the parameter was constant for any size of larvae without taking the strike distance into account (Table 2). However, the assumption of a constant precision parameter is reasonable given that larger larvae are more successful in their strikes.

Capture success with prey escape response

We couple the strike precision of the larva with a prey escape response as in Fiksen and Mackenzie (2002) (Fig. 2). The prey escape angle θ is drawn from a normal distribution with mean 30º and 30º of standard deviation (Titelman 2001; Fiksen and MacKenzie 2002).

We limit the jump of the larva in the strike x* to j/2 as in Fiksen and Mackenzie (2002). This means that the time that the larva needs to arrive at τ_{max} is the time frame for successful attack:

$$\tau_{\max} = \frac{r_s + x*}{v_a \cos\alpha}, \tag{3.2}$$

where r_s is the strike distance, v_a is larval attack velocity (Table 2). We calculate the time it takes for the larva and the prey to be in the same place along the x coordinate, assuming that the prey will make an escape jump in the moment the strike start (Caparroy et al. 2000; Titelman 2001):

$$\tau = \frac{r_s}{v_a \cos\alpha - w\cos\theta} \tag{3.3}$$

If τ is longer than the time frame τ_{max} then prey escapes. But if τ is smaller than the time limit $\tau_{max,}$, then the distance z_{lp} between larvae and prey at τ is:

$$z_{lp} \leq v_a \tau \sin\alpha - w\sin\theta \tag{3.4}$$

If the prey is inside the mouth area at this time then the capture is successful [Eq. (3.1)]. We calculate the capture ability success $Pca_{i,j}$ for a given size of larva j and prey size and escape velocity i, running $Nsim$ = 1000 simulations of larval attack with stochastic angle α and stochastic prey escape angles θ.

$$Pca_{i,j} = \frac{\sum_{k=1}^{Nsim} x_k}{Nsim}, \quad x_k = \begin{cases} 1 & z_{lp,k}|\alpha_k,\theta_k) \leq (m_j - dp_i)/2 \\ 0 & z_{lp,k}|\alpha_k,\theta_k) > (m_j - dp_i)/2 \end{cases} \tag{3.5}$$

where k is the simulation index, $z_{lp,k}$ is the distance

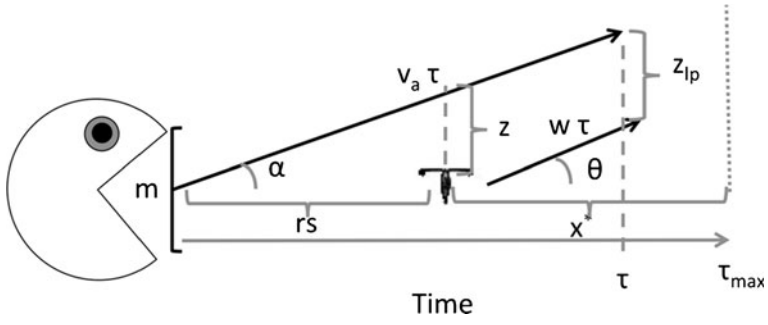

Fig. 2 Schematic drawing of a larva attacking a prey, where m is the mouth size, α is the angle of the jump of the larva, θ is the angle that prey choose to escape, r_s is the strike distance, v_a is the larval velocity, w is prey's velocity, z is the distance between larva and prey with no escape behavior (see text), τ is the time when larva and prey are in the same place in the x coordinate, z_{lp} is the distance between larva and prey at the time τ and τ_{max} is the maximum time at which larva can capture the prey

Table 2 Parameter's and variable's description, unit, value or source and reference of the capture success model

Symbol	Description	Unit	Value, source	Ref
j	Standard length of the larva	m		
m	Larval mouth width	mm	m_j=0.0543+34.5 j	(1)
$r_{s,}$	Strike distance	m	0.07× j	(1)
σ	Strike precision parameter	m	6×10^{-5}	(2)
z	Vertical distance between larval mouth and prey with no escape behavior	m	$N(0,\sigma^2)$	(2)
α	Attack angle	°	$\arctan(z/r_s)$	
θ	Prey escape angle	°	$N(30,30^2)$	(3)
τ	The time for larva to align with prey	s	Eq. (3.3)	
x*	Maximum jump distance	m	j/2	(4)
τ_{max}	Duration of one strike	s	Eq. (3.2)	
v_a	Attack velocity	m	8× j (see text)	
w	Prey escape velocity	m/s	$(0\text{-}10lp\text{-}50lp\text{-}100lp)\times10^3$	

(1) (Hunter 1977), (2) (Beyer 1980), (3) (Titelman 2001), (4) (Fiksen and MacKenzie 2002)

between larva and prey in the simulation k and $\alpha_{k\ \text{and}}$ and θ_k are the larval attack and prey escape angle in the simulation k.

Bioenergetic model

The details of the bioenergetic model are described in Urtizberea et al. (2008). The model was parameterized with field and experimental data of the anchovy larva *E. mordax*. The gut content depends on the amount of mass ingested and digested. In the model the amount of mass digested is limited by gut content or temperature and used for growth and metabolic cost (Fig. 1). If the larva is not food limited, the larva will attain maximum growth potential which increases linearly with temperature and it does not change with size [see equation 9 in Urtizberea et al. (2008)]. The assimilation efficiency and the gut size are size dependent functions.

Prey size spectra

The biomass size spectra describe the distribution of prey biomass across logarithmically equal size classes of prey width. The size spectra are normalized by dividing the biomass of each prey size class by the width of the class (Platt and Denman 1978). This makes the size spectra independent of the length of the size class. The normalized biomass-size (NB-S) spectra fits a linear relationship between the logarithm of normalized biomass and prey size (Platt and Denman 1978):

$$\frac{B_i}{\Delta dp_i} = e^a dp_i^b \tag{4}$$

where Δdp_i is the length range of prey size class i, dp_i is the geometric mean width of size class i which is equivalent to the mean of the size class in logarithmic scale, B_i is the prey biomass in size class i (expressed as mg dry weight m^{-3}), b the slope and a the intercept of the linear relationship. The normalized size spectra between biomass and prey size have been estimated for different areas of the Bay of Biscay, giving slopes between −2 and 0 (Irigoien et al. 2009). In this study, prey abundances are estimated using theoretical normalized size spectra with slopes within the range of those found in the field (Fig. 3).

During the spawning period of anchovy larvae in the Bay of Biscay, Irigoien et al. (2009) estimated biomass of zooplankton between 0.1 and 0.4 mm width to be between 4 and 15 mg C m^{-3}. Assuming that carbon content is 40 % of the dry weight (Champalbert et al. 1973), the zooplankton biomass for the same range is between 10 and 37.5 mg dw m^{-3}. In order to calculate the biomass for each size class using 3 different slopes (−2, −1, 0), we fixed the total biomass, *TB,* at 20 mg dw m^{-3} for prey width between 0.025 and 0.4 mm (Table A1, see supplementary material). We also calculated the prey size distribution for prey width between 0.025 and 0.8 mm (Table A2, see supplementary material) in order to compare the effect of the same slope and total biomass in different prey range.

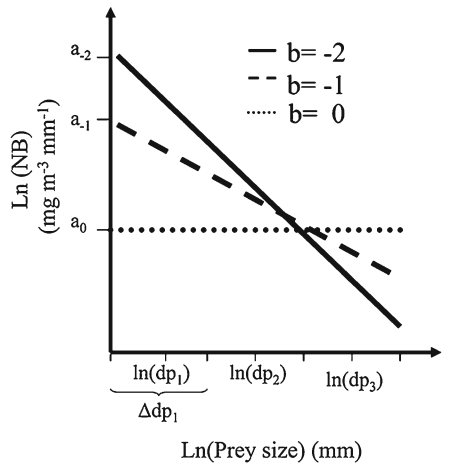

Fig. 3 Normalized biomass size spectra between biomass and prey size. The parameter a_i is the intercept estimated when the slope, b, is equal to i: −2, −1, 0. The parameter dp_i is the nominal value of the prey size class Δdp_i

We focus on the feeding behaviour of early anchovy larva between 4 and 8 mm. The mouth width of an 8 mm anchovy larva is 0.33 mm (Hunter 1977) and the minimum prey width found in the European anchovy larva gut is 0.027 mm (García and Palomera 1996; Conway et al. 1998; Catalán et al. 2010; Morote et al. 2010; Tudela et al. 2002). We divide the total biomass among n=4 prey size classes in base 2 logarithmic bins: 0.025–0.05; 0.05–0.1; 0.1–0.2; 0.2–0.4 mm (Table A1, see supplementary material). To assess the sensitivity of the model to the prey size range we add another prey size class in the interval 0.4 to 0.8 mm. Then we divide the total biomass into 5 prey size classes ranging from 0.025 to 0.8 mm (Table A2, see supplementary material).

To find the total biomass TB in a given size range we first rearrange Eq. 4 and sum over all prey sizes classes n:

$$TB = \sum_{i=1}^{n} B_i = e^a \sum_{i=1}^{n} dp_i^b \Delta dp_i. \quad (4.1)$$

Then we calculate the value of a and the biomass of each size class for a given total biomass and slope, b:

$$a = \ln\left(\frac{TB}{\sum_{i=1}^{n} dp_i^b \Delta dp_i}\right). \quad (4.2)$$

To test the sensitivity of larval ingestion to the number of size classes, we introduced subclasses within each size class. There are 15 subclasses in total, and they all have length intervals of 0.025 mm (Table A3, see supplementary material). Thus, the size class from 0.025 to 0.05 mm has one subclass, and there are two subclasses from 0.05 to 0.1 mm, four subclasses from 0.1 to 0.2 mm, and eight subclasses from 0.2 to 0.4 mm. The biomass in a size class is divided equally between its respective subclasses, meaning that subclasses within a size class have the same biomass.

The relationship between prey length, lp_i (mm), and width, dp_i (mm), was estimated for the geometrical mean width of each size class. The prey length and width relationship was estimated from prey found in the gut of larval anchovy (Conway et al. 1998):

$$lp_i = 2.57dp_i - 0.052, \quad (r^2 = 0.76, n = 8) \quad (4.3)$$

Anchovy larvae *E. encrasicolus* mainly feed on nauplii, copepodites and eggs (Conway et al. 1998; Tudela et al. 2002), so the dry weight of each size class was estimated from a general relationship for zooplankton (Peters and Downing 1984):

$$wp_i = 9.86lp_i^{2.1}, \quad (4.4)$$

where wp_i is the estimated prey weight in μg dw. Then the ratio between biomass and individual weight in each size class is the abundance of prey in each size class.

Model simulations

Calibration and sensitivity analysis on capture success

We calculated the capture success of larvae between 4 and 11 mm for a prey from 0.035 mm to 0.4 mm width. The escape velocity of more evasive prey species is between 20 and 200 prey lengths/s (Mauchline 1998; Titelman 2001), thus, we calculated the capture success with prey of different escape velocities (no escape, 10, 50, 100 prey length/s).We ran the model for 1000 attack for each larval and prey length with larval jump angle chosen randomly (z) from a normal distribution with mean 0 and σ^2 variance and prey escape angle θ is drawn from a normal distribution with mean 30º and 30º of standard deviation.

Hunter (1977) reported strike distance for anchovy larvae that were approximately 7 % of larval length, however, we did a sensitivity analysis for the capture

success of larvae with strike distance of 5 % and 16 % reported previously for juvenile stickleback and cod larvae (Viitasalo et al. 1998; MacKenzie and Kiørboe 2000).

Hunter (1972) estimated, from laboratory experiments, that larval anchovy attack or strike velocity increases with length nonlinearly, however the estimates were close to one body length/s and the burst speed, measured when larvae is swimming continuously beating the tail and body from side to side, was close to 15 larva body length/s. We made a sensitivity analysis of attack velocity and compared capture success when the attack velocity is 1, 8 and 15 larval body length/s.

We also did sensitivity analysis of capture success with different maximum distance that larva jump in one strike (x^*) 1, 0.5, and 0.2 larva length.

Conical vs. hemispherical perceptive volume in a turbulent environment

We found the clearance rate for different prey sizes given a larva with a hemispherical (C_M=6 would be for spherical, and C_M=6×0.8 for hemispherical) or a conical (C_M=6×0.2) perceptive volume [Eq. 2; and see Pécseli and Trulsen (2007)] with an opening angle of 26° (Hunter 1972).

Optimum prey size

What is the effect of turbulence for ingestion at different prey size? To answer this we calculate the ingestion rate of anchovy larvae at different prey size with different turbulence level. We assume a prey abundance of 5000 prey m^{-3} for each prey size, and define the optimum prey size as one yielding highest biomass consumption. We did a sensitivity analysis on handling time and compared the predictions with constant handling time (Table 1) and handling time increasing with prey length (Walton et al. 1992).

The slope and resolution of size spectra

How does prey size structure affect the feeding success of 4 mm and 8 mm larvae? For a given larva with a hemispherical perceptive volume we calculate the prey abundance for each prey size class when the slope of the NB-S spectra is −2, −1 and 0. We assume a total biomass of 20 mg dw m^{-3} distributed in two different prey size ranges from 0.025 to 0.4 mm (Fig. 4a) and from 0.025 to 0.8 mm (Fig. 4b). In addition, we analyze the effect of prey size class resolution on the ingestion rate by comparing it to the prey abundance from 0.025 to 0.4 with 15 linearly distributed prey size classes for each slope in the NB-S spectra (Fig. 4c). If the slope is 0, the normalized biomass is the same for any size of prey, while the biomass in the prey size class increases with size (Table A1, see supplementary material). If the slope of the NB-S spectra is −1 then the biomass is the same for each size class, and if the slope is −2 then the biomass decreases with size class. From biomass per size class we find the abundance of each prey category; steeper slopes increase the prey abundance ratio from small to large prey (Table A1, see supplementary material). We tested the sensitivity of predictions to size class

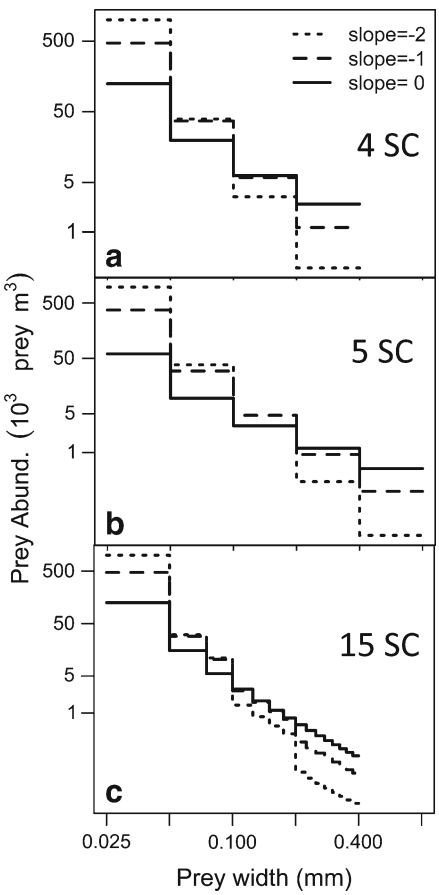

Fig. 4 Estimated prey abundance from NB-S spectra and total abundance of 20 mg dw m^{-3} in the range (**a**) from 0.025 to 0.4 mm divided into four logarithmic scale (base 2) size classes (SC), (**b**) from 0.025 to 0.8 mm divided into 5 logarithmic scale (base 2) SC and (**c**) from 0.025 to 0.4 mm divided into 15 size classes of the same width interval of 0.025 mm. The *lines* represent the calculated abundance in each prey size class with different slope in the NB-S spectra

resolution: one with four size classes in logarithmic base 2 (Table A1, see supplementary material) and the other with 15 linearly distributed prey size classes (Table A3, see supplementary material).

Growth at different temperatures and prey biomass

We calculate the specific growth of a 4 mm larva at different temperature from 10 to 25 °C and total prey biomass assuming a slope of −1 in the NB-S spectra and with abundance or biomass of prey at each size class increasing at the same rate. We compare the results for a larva with hemispherical and conical shaped perceptive volume.

Results

Calibration and sensitivity analysis on the predictions of capture success

Hunter (1972) described the feeding success with age, and predicted capture success when prey has no escape behaviour are similar to estimated capture success from laboratory experiments with prey of very low motility, such as *Brachionus* (0.133 mm width) and *Artemia* (0.236 mm) (Hunter 1972) (Fig. 5). The conversion to size was done from the size-age relationship in Theilacker (1987).

The escape is more effective for larger prey (Fig. 6). The capture success is sensitive to the attack precision of the larva. Prey with escape velocity of 10 length prey/s and no escape is almost the same when larval jump precision σ=0.06 mm. Nevertheless, when σ=0, then the capture success is lower for the large larvae with 10 length prey/s than for prey that do no escape.

The calculated capture success is sensitive to predator prey size ratio, strike distance (Fig. 7a) and the escape velocity (Fig. 7b) of the prey (Mauchline 1998). We assume an attack velocity of 8 larva length/s. The capture success is not sensitive to maximum capture distance x*.

Conical and hemispherical perceptive volume in a turbulent environment

Since the visual range increases with prey size, the clearance rate of a larva with large prey is higher

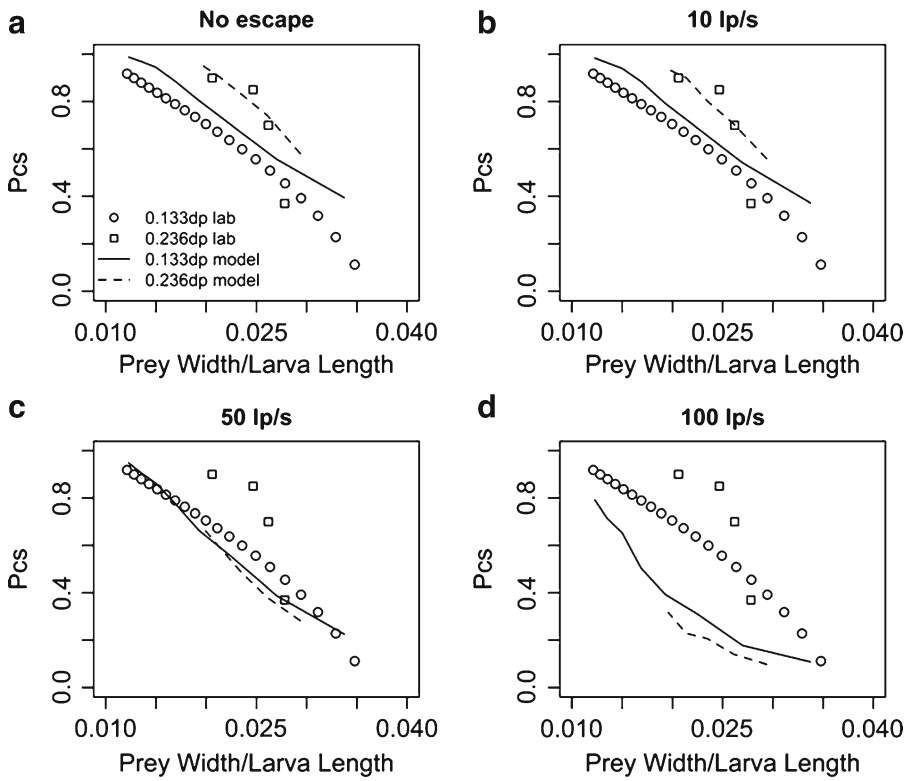

Fig. 5 The points and squares are the estimated capture success (*Pcs*) from laboratory experiments of larvae of different lengths trying to capture a *Brachionus* prey of 0.133 mm prey width (*dp*) and 0.236 mm prey width (*dp*) *Artemia* (Hunter 1977). The full (*Brachionus*) and broken (*Artemia*) *line* are the capture success from the model for (**a**) prey without escape behaviour (no escape), (**b**) with an escape velocity of 10 (**c**) 50 and (**d**) 100 prey lengths/s. The capture success is calculated by simulating for each larval size and prey, 1000 larval attack with stochastic attacking angles α and stochastic prey escape angles θ. We assume σ is 0.06 (see text)

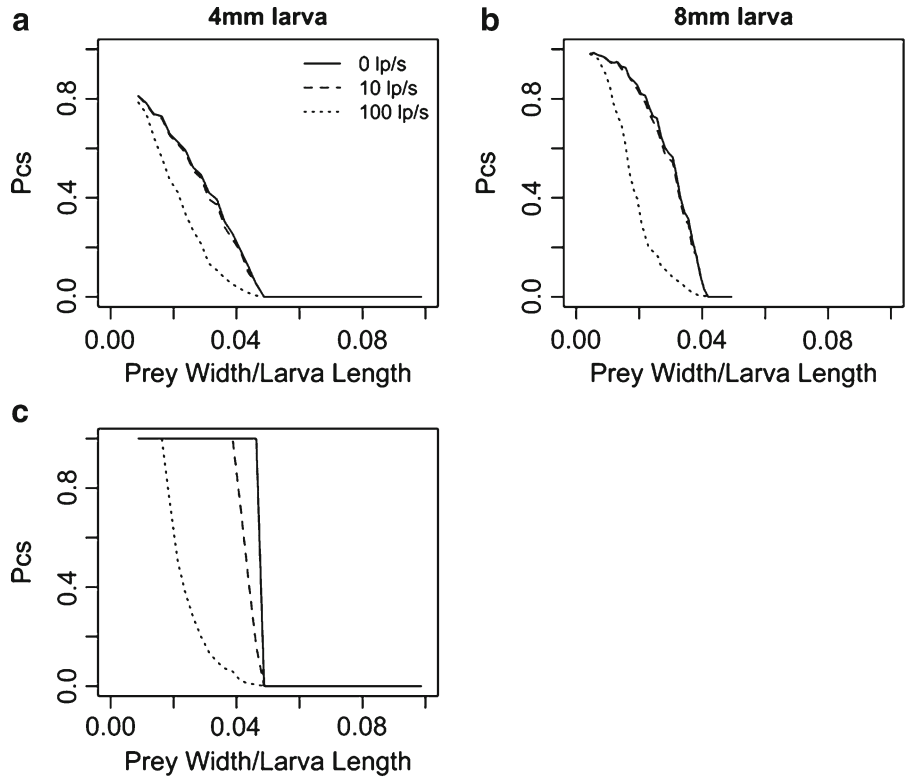

Fig. 6 Capture success (*Pcs*) of a larva of (**a**) 4 mm and (**b**) 8 mm with increasing prey size. The *lines* describe the capture success of prey with different escape velocity: 0 (*line*), 10 (*broken line*) and 100 (*dotted line*) length prey per second (prey lengths/s). The larvae have an error sigma =0.06 (top panels) or no error sigma = 0 (**c**)

(Fig. 8a). The clearance rate between larva and prey increases noticeably with turbulence at levels above $10^{-6}\,m^2\,s^{-3}$ (Fig. 8a and b), because turbulence becomes dominant relative to larval fish swimming speed. The clearance rate of a larva with a hemispherical perceptive volume is about 5–10 times higher than for a larva with a conical perceptive volume.

Pursuit success decreases with increasing turbulence (Fig. 8c). Therefore the capture success; defined as the product of capture ability and pursuit success, also decreases with turbulence and approaches zero at turbulence levels above $10^{-6}\,m^2\,s^{-3}$ (Fig. 9a). The increase on escape velocity of the large prey reduces the capture success of the larva (Fig. 9b).

Optimum prey size

The optimum prey size ratio (prey width and larva length) is close to 4 % of larva size when prey has no escape behaviour (Fig. 10a) and it decreases with prey escape velocity; to 3 % when larval escape velocity is 100 length prey/s (Fig. 10b). The relative optimum prey size does not change either with size and is not sensitive to handling time.

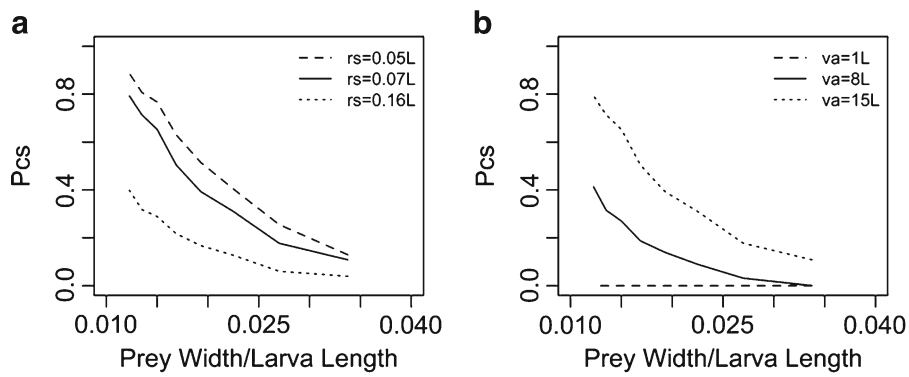

Fig. 7 **a** Sensitivity analysis on capture success (*Pcs*) with different strike distances (r_s) 5 % (*discontinuous*), 7 % (*continuous*) and 16 % of larval length (*L*) (*dotted*) and prey escape speed 100 prey lengths/s. **b** Sensitivity analysis on capture success with different attack velocities (v_a): 8 (*continuous*), 1 (*discontinuous*) and 15 (*dotted*) larva body length per second, *L/s*

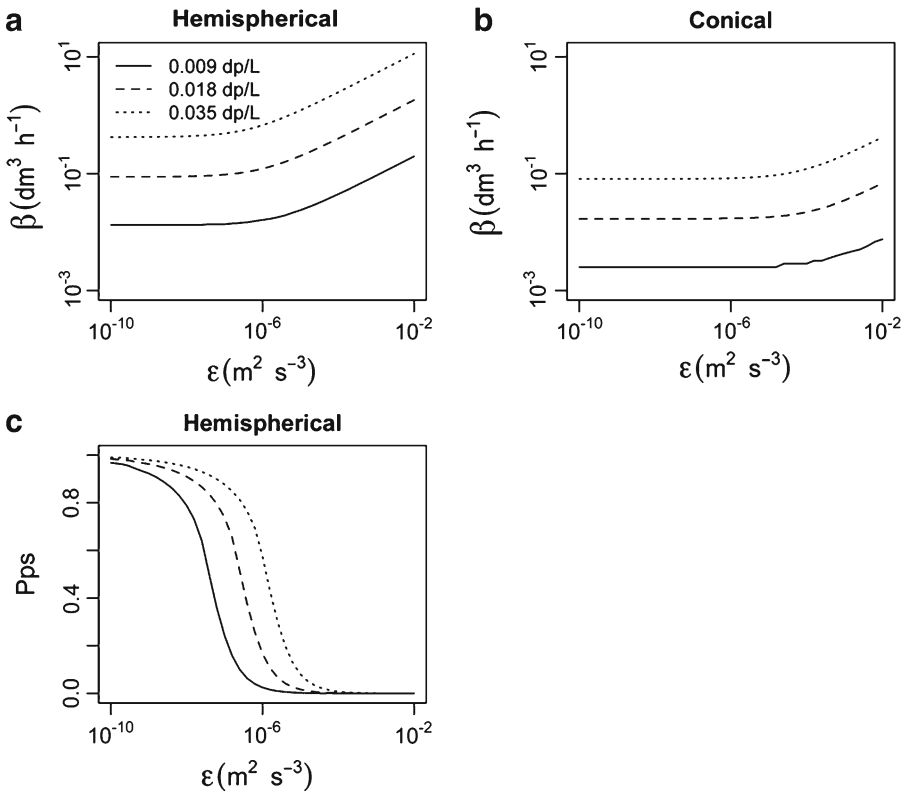

Fig. 8 Modelled clearance rate, β, of a 4 mm larva at different turbulence levels, ε: (**a**) assuming a hemispherical perceptive volume (90° of the opening angle of the cone, C_M=6×0.8) and (**b**) assuming a cone shaped perceptive volume (26° the opening angle of the cone, C_M=6×0.2). Predicted pursuit success (*Pps*) assuming (**c**) a hemispherical perceptive volume. The *lines* represent different prey size in terms of prey width to larva length ratios (prey width/L) = 0.009, 0.018, and 0.035, for a larva with 4 mm

The slope and resolution of size spectra

For a 4 mm larva at calm conditions, the ingestion rates with different prey size structures are quite similar and does not change at turbulence below 10^{-7}m^2 s^{-3} because at low turbulence level the encounter is dominated by larval swimming speed and at higher turbulence level the ingestion decreases (Fig. 10a) due to the low pursuit success. (Figure 11a). The lowest ingestion rates are predicted when the slope is 0, since the abundance of the optimum prey size is lower. An 8 mm larva attains the highest ingestion rates when the slope is 0 at any turbulence level (Fig. 11b), because slope 0 gives the highest biomass of the optimum prey size class for an 8 mm larva. However, if we assume the same total biomass in a larger prey size range from 0.025 to 0.8 mm (Fig. 11b), the ingestion rate at different prey size structure changes (Fig. 11c). In this case, a 4 mm larvae will have half the ingestion rate at 0 slope compared to that of the steeper slopes (−1 or −2) (Fig. 11c). At this prey size range there are significant differences in the ingestion rates of a 4 mm larva due to

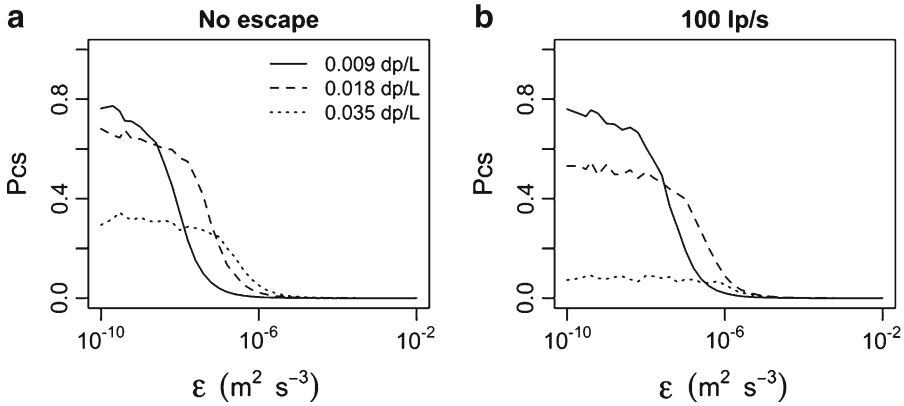

Fig. 9 Predicted capture success (*Pcs*) (multiplication of pursuit and capture ability) at different turbulence levels, ε, assuming a hemispherical perceptive volume and (**a**) no prey escape behaviour and (**b**) with prey escape velocity of 100 prey lengths/s. The *lines* represent different prey size in terms of prey width to larva length ratios = 0.009, 0.018, and 0.035 prey width/L

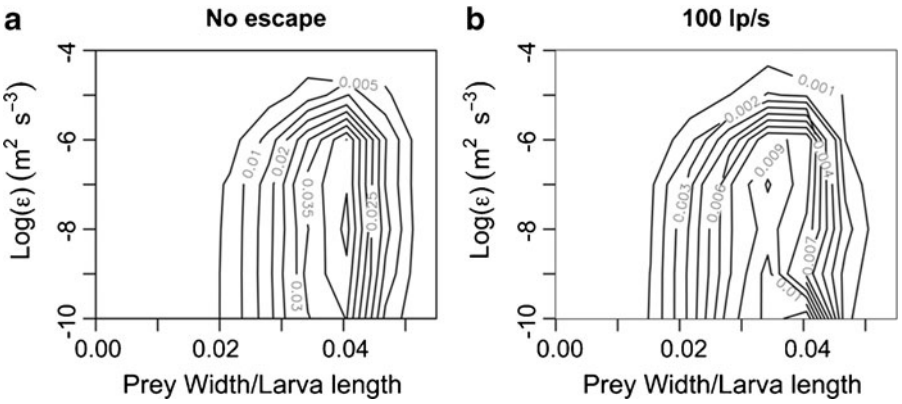

Fig. 10 At satiated light conditions ingestion rate per hour of different prey size ratio under different level of turbulence, ε, for a 4 mm larva. Assuming prey with no escape behaviour (**a**) and prey with escape velocity of 100 prey lengths/s (**b**). We assumed the same abundance of prey at any prey size ratio (5000 prey m^{-3}) and larva with hemispherical perceptive volume (90° of the opening angle of the cone)

the prey size structure (Fig. 11c). We see the same effect for the 8 mm larva (Fig. 11d). In this case, the optimum prey size structure for 8 mm larva is at a steeper slope (−1) than before. If the same biomass pertains to a larger size range, the biomass in the smallest prey size class decreases. The decrease in the smallest prey size is higher for a prey size structure with slope 0 than with steeper slopes (Fig. 11e). Therefore, the prey size structure with steeper slopes gives the highest ingestion rates when the maximum prey size included in the study is further from the optimum prey size of the larva. However, we can conclude that feeding is sensitive to the abundance of a particular prey and therefore it is sensitive to the slope of the prey size spectra. In terms of the NB-S spectra, this means that a small larva benefit from a prey size structure with steep slope while a large

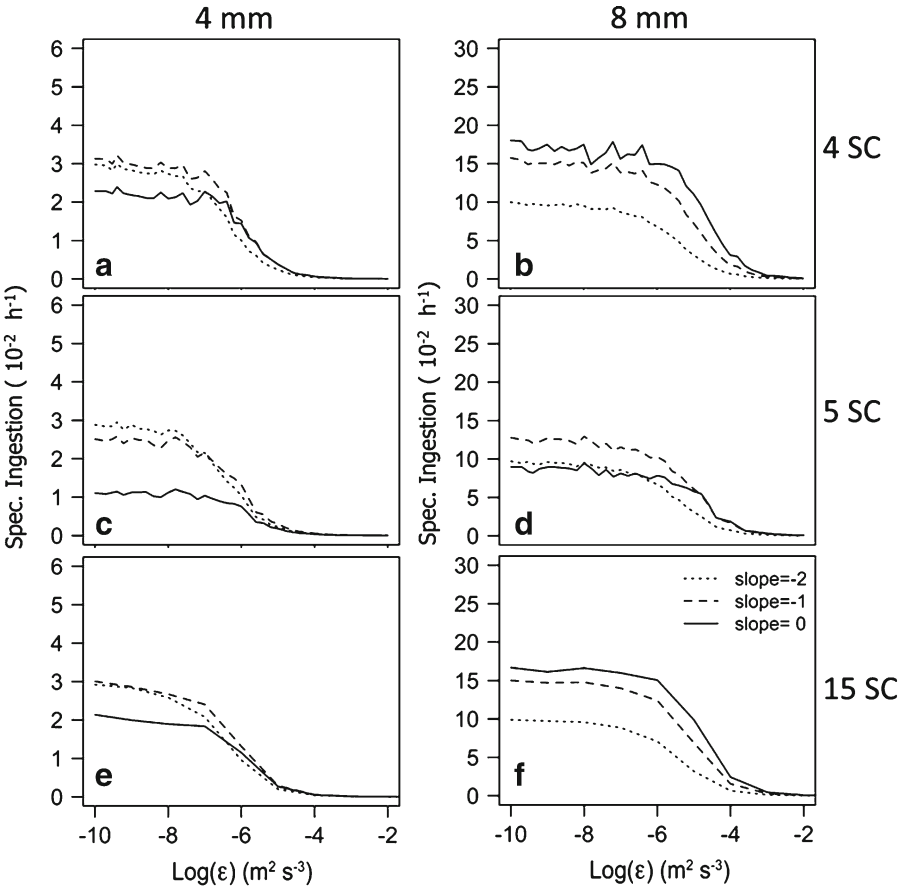

Fig. 11 Left and right panels show the specific ingestion rates per day for 4 and 8 mm larvae assuming 100 prey lengths/s prey escape velocity at different turbulence levels, ε, with 4 size classes (**a** and **b**), with 5 size classes (**c** and **d**) and with 15 size classes (**e** and **f**). The *lines* represent the estimated ingestion rates with different prey size structure defined by −2, −1 or 0 in the slope of the NB-S spectra

larva benefit from less steep slopes. In addition the large larva has better visual capacity and therefore it sustains the maximum ingestion rate at higher turbulence level than the smaller larvae (Fig. 11f).

The total ingestion rate of a 4 mm and 8 mm larva give similar results for both resolutions of size classes, logarithmic base 2 (4 size classes) or lineally distributed (15 size classes) (Fig. 11a, b, e, f). In general, it appears from Fig. 11 that the foraging success of a larva is not very sensitive to the prey field resolution. The ingestion rate in both resolutions is dome-shaped with prey size for all slopes (Fig. 12a, b). When the slope is steeper (−2), most of the mass ingested is shifted toward the smallest prey (Fig. 12b).

The ingestion decreases with turbulence because the smallest prey size class is more difficult to capture. The mean prey size ingested increases with turbulence (Fig. 13) and total ingestion decreases faster with turbulence when the prey size distribution has steeper slope (prey field is more dominated by small prey).

Growth at different temperatures and prey biomass

The prey biomass that larvae required in order to get the maximum growth rate increases linearly with temperature (Fig. 14a). A larva with hemispherical perceptive volume required around 20 mg dw m^{-3} of total prey biomass at 20 °C while a larva with a conical perceptive volume require around 100 mg dw m^{-3} (Fig. 14b). The amount of prey biomass required for a larva with a hemispherical perceptive volume is reasonable when comparing with the prey biomasses observed in the field.

Discussion

The models developed by Galbraith et al. (2004) and Lewis and Bala (2006) showed that the increase in encounter rate with turbulence is lower for a larva with a wedge shaped (similar to a cone shaped but the vertical section is a square instead of circle) than for a larva with a hemispherical perceptive volume. Mariani et al. (2007) developed an object-oriented numerical model for cod larvae with pause-travel search strategy and estimated ingestions at turbulent levels relevant for larvae with hemispherical and wedge shaped perceptive volumes. Their results showed that the increase in ingestion with turbulence was lower for a wedge shaped perceptive volume, but in both cases the foraging success was dome-shaped with turbulence. However, laboratory experiments and theoretical models suggest that the increase in encounter rate due to turbulence is lower for a larva with cruising swimming behaviour like herring (*Clupea harengus*) than for a larva with pause-travel search strategy like cod (*Gadus morhua*) (MacKenzie and Kiørboe 1995; Fiksen et al. 1998). Our model predicts that the turbulence does not increase the ingestion rate of anchovy larva assuming cruissing swimming behaviour. Mackenzie (2000) made a review of field studies analyzing the effect of turbulence on fish larvae. Here different studies on anchovy larvae show that the gut content or growth does not increase with turbulence (Lasker 1975; Owen et al. 1989; Clemmesen et al. 1997; Conway et al. 1998). In our model the negative effect of turbulence (at high

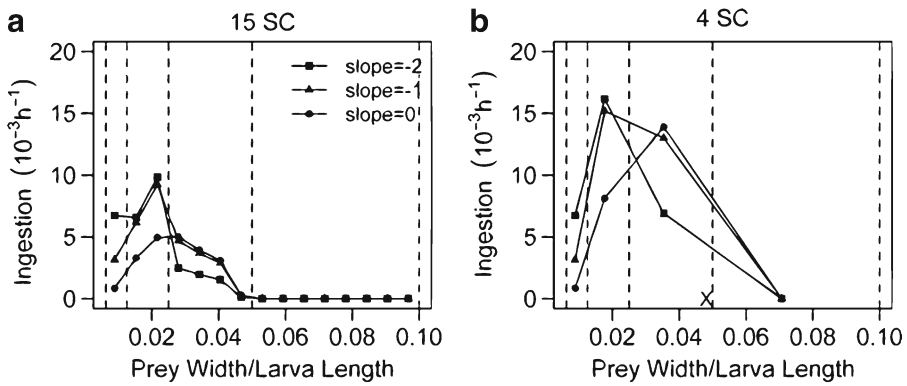

Fig. 12 The ingestion rates of 4 mm larvae are modelled at 15 prey size classes of fixed intervals (**a**) and at four size classes in base 2 logarithmic scale intervals (**b**). The ingestion rate is found at calm conditions (low turbulence) of different prey size with 20 mg dw m^{-3} and different slopes in the normalised size spectra: −2, −1 and 0. The *broken lines* represent the interval of the size classes in the logarithmic scale and the cross the mouth size of a 4 mm larva

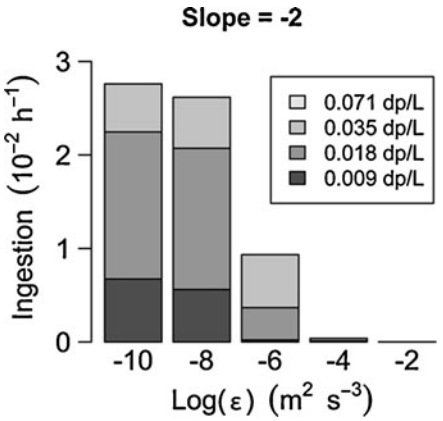

Fig. 13 The modelled specific ingestion rate per hour of a 4 mm larva at each prey size assuming an escape velocity of 100 prey lengths/s at different turbulence level when the slope of the NB-S spectra is −2. The colours represent the fractions of total ingestion rate at each turbulence level and each prey size class relative to larva size: 0.009, 0.018, 0.035 and 0.071 prey width/L

turbulence levels) is caused by the small perceptive volume of anchovy larvae and the low capture success of large prey; even if the average prey size increases at high turbulence levels, the total ingestion decreases.

Laboratory experiments with northern anchovy larvae (*E. mordax*) suggest that anchovy larvae have a cone shaped perceptive volume of 26º (Hunter 1972). When cone shaped perceptive volume is assumed in our model, the prey density needed to obtain maximum growth rate or even to survive is higher than what is estimated in the field. Lasker (1975) in the 'stable ocean hypothesis' suggested that anchovy larval survival depends on high prey concentrations and he found that those high prey concentrations in the field were aggregated in patches in stratified waters at calm and stable conditions. But in the field, prey densities are estimated assuming homogeneous prey distribution in the entire water column while sampling on the submeter scale showed that prey could be aggregated in patches (Owen et al. 1989). However, laboratory observations suggest different visual perceptive volumes between clupeoid fish larvae. Rosenthal and Hempel (1970) suggest herring larvae (*Clupea harengus*) have a quarter-sphere volume. *Anchoa mitchilli* larvae may have a wedge shape perceptive volume, where the opening angles differ in the horizontal and vertical plane, 25º in the vertical plane and 60º in the horizontal plane (Chesney 2008). In addition, taking the tip of the snout as reference in the vertical plane, 0º, *Anchoa mitchilli* mainly forage between 20 and 70º (Chesney 2008), while northern

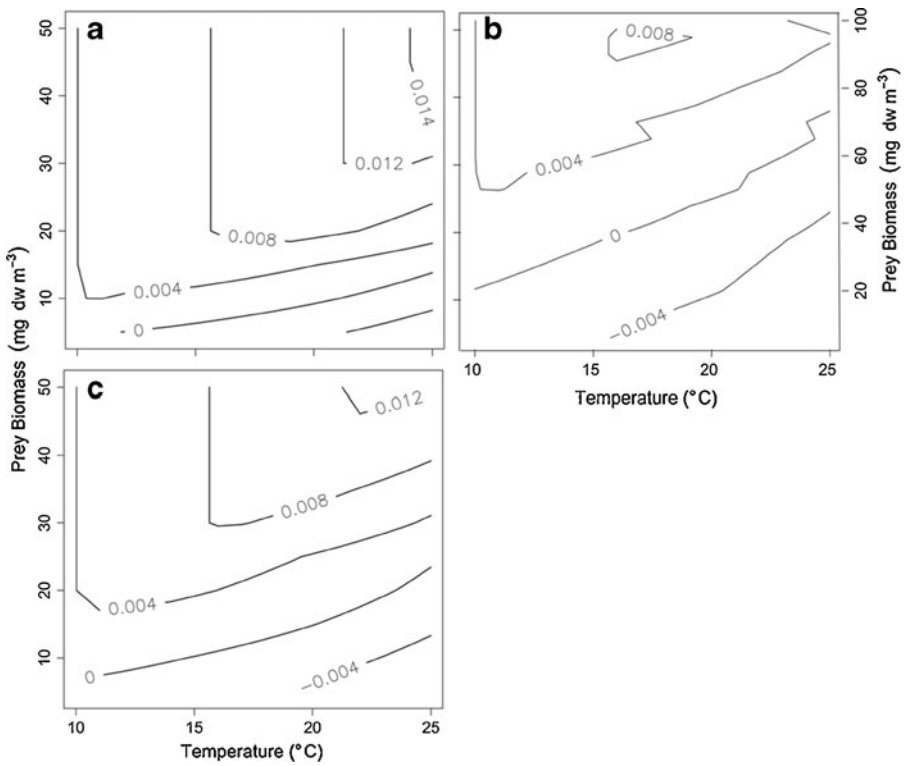

Fig. 14 Simulated specific growth rate ($\mu g \mu g^{-1} h^{-1}$) assuming prey escape velocity of 100 prey lengths/s for (**a**) a larva with a hemispherical perceptive volume (90° of the opening angle of the cone), and (**b**) with cone shaped perceptive volume (26° of the opening angle). Both as functions of temperature and total prey biomass, and assuming slope −1 in the NB-S spectra with 4 size classes. (**c**) Assuming hemispherical perceptive volume and assuming that larvae do not feed in the smallest prey size class when the slope in the NB-S spectra is −1

anchovy mainly feed between −26 and 26º (Hunter 1972). Laboratory experiments also show that the average perception distance and swimming speed decreases with increasing prey densities (Munk and Kiørboe 1985) and increases with turbidity (Chesney 2008). Anchovy larvae, at the stage of first feeding, have already developed olfactory organs (O'Connell 1981), and feeding is influenced by chemosensory processes (Knutsen 1992; Kolkovski et al. 1997).

The representation of foraging behaviour of larva fish requires some characterization of prey size distribution. Size spectra is a common description of biomass distribution across prey size classes and it enables fast estimates of biomass size spectra in the field (Ashjian et al. 2001; San Martin et al. 2006; Zarauz et al. 2007; Irigoien et al. 2009) due to its simplicity and novel innovations in image analysis (Grosjean et al. 2004; Davis et al. 2005; See et al. 2005). The slope of the size spectra refers to the change in biomass distribution across prey size classes. The division of biomass in prey size classes is made on a logarithmic scale in base 2. Firstly because of limitation of sampling techniques in larger prey and secondly because the double logarithm transformation of the normalized biomass and prey size classes at these scale fits a linear relationship (Blanco et al. 1994). Nevertheless, there are some particular cases where the zooplankton community is not in a steady state and the biomass spectrum deviate from linearity (Nogueira et al. 2004; Sourisseau and Carlotti 2006; Zhou 2006). In this case, the slope and intercept of the NB-S spectra would not be appropriate to describe the prey size distribution in the field.

There are a few laboratory studies exploring larval ingestion in response to different prey size distribution (Munk 1992; Seljeset et al. 2010) but none with anchovy larvae. Thus, it is very difficult to find relevant data to calibrate the foraging model developed here. On the other hand, field studies analyzing anchovy larval feeding behaviour often measure size of ingested prey, but not prey preferences in terms of size. The model predicts highest ingestion rates with the prey size distribution that maximize the abundance of the optimum size of prey. The optimum prey size (width) predicted by the model is 3 % of larval length (or prey length between 6 and 7 % of larval length) when we assume prey escape velocity of 100 prey length/s. The preferred prey size (length) estimated from field data for herring larvae was 3 % of larval length while for cod larvae was 5 % of larval length (Munk 1992, 1997). Anchovy and herring larval mouth width and behaviour is very similar, so we could expect similar optimum prey size for both, nevertheless the estimated preferred prey size of herring larvae is half to the prediction of our model for anchovy larvae. In the field, the maximum prey width ingested by anchovy larvae *E. encrasicolus*, between 3 and 10 mm in the Mediterranean sea, is close to the optimum prey size (width) predicted by the model 2 and 3 % of larval size (or prey length 7 % of larval length) (see Conway et al. 1998, Fig. 5; see Tudela et al. 2002, Fig. 2). This could suggest that our model overestimates the optimum prey size of anchovy larvae.

The role of small prey in the feeding or survival of larvae in the sea is unknown (de Figueiredo et al. 2005, 2007). We calculated the specific growth of a 4 mm larva assuming it does not feed on them when the slope of the NB-S spectra is −1 (not shown). The model suggests that feeding or not feeding on the smallest prey size class results in similar specific growth rate when the slope is −1 (not shown). We also calculate the specific growth rate assuming a 4 mm larva does not feed on prey larger than 2 % of its size (in terms of prey width) (Fig. 14c). The result suggests that larval growth is most sensitive to the feeding success on largest prey since anchovy larva would require higher prey biomass in order to survive or obtain maximum growth rate.

In the Bay of Biscay, anchovy (*E. encrasicolus*) spawn in spring; mainly in the river plumes of Gironde and Adour and at the shelf break (Motos et al. 1996). Despite the fact the total mesozooplankton biomass is higher above than outside the shelf, large anchovy larvae are still found off the shelf (Irigoien et al. 2008). Recent studies have reported the spatial distribution of zooplankton size spectra in spring from 1998 to 2006 in the Bay of Biscay (Zarauz et al. 2007; Irigoien et al. 2009). Irigoien et al. (2009) found that the slope of the NB-S spectra were less steep with increasing distance to the coast, meaning that the biomass of large organisms is higher relative to the abundance of small prey over the shelf. Consequently, the anchovy larvae will experience different food conditions depending on where they are advected. Our results show that the optimum prey size structure changes with size and the largest larva have highest ingestion rate at less steep prey size structures.

Therefore while the larva is getting larger, its optimum prey size structure is found at increasing distance to the coast. However, not only the prey size structure changes with distance to the coast, but also the total prey biomass. Potential differences in feeding conditions between offshore and inshore areas depend on both prey size structure and prey biomass.

The models described here are purely mechanical, and we end by pointing out that there is considerable potential for larvae to modify their foraging success through behavioural flexibility, for instance in the search rate or vertical positioning [see (Fiksen and Jørgensen 2011)]. Larvae feeding in size-spectra may also perform optimal foraging decisions involving not to pursue particular prey sizes (Visser and Fiksen 2012). Such models still need realistic representation of the processes involved in prey encounters and capture success, which has been the primary focus here.

Acknowledgments We would like to thank to A.F Opdal, N. Dupont and L. Zarauz for their useful comments in the manuscript, and the Norwegian Research Council for financial support. This paper is contribution no. 608 from AZTI Foundation (Marine Research).

References

Aksnes DL, Giske J (1993) A theoretical model of aquatic visual feeding. Ecol Model 67(2–4):233–250

Aksnes DL, Utne ACW (1997) A revised model of visual range in fish. Sarsia 82(2):137–147

Ashjian CJ, Davis CS, Gallager SM, Alatalo P (2001) Distribution of plankton, particles, and hydrographic features across Georges Bank described using the Video Plankton Recorder. Deep-Sea Res II 48(1–3):245–282

Beyer JE (1980) Feeding success of clupeoid fish larvae and stochastic thinking. Dana 1:65–91

Blanco JM, Echevarria F, Garcia CM (1994) Dealing with size-spectra: some conceptual and mathematical problems. Sci Mar 58:17–29

Caparroy P, Thygesen UH, Visser AW (2000) Modelling the attack success of planktonic predators: patterns and mechanisms of prey size selectivity. J Plankton Res 22 (10):1871

Catalán IA, Folkvord A, Palomera I, Quílez-Badía G, Kallianoti F, Tselepides A, Kallianotis A (2010) Growth and feeding patterns of European anchovy (Engraulis encrasicolus) early life stages in the Aegean Sea (NE Mediterranean). Estuar Coast Shelf Sci 86(2):299–312

Champalbert G, Gaudy R, Kerambrun P (1973) Résultats préliminaires sur la composition chimique élémentaire comparée en carbone, hydrogène et azote de quelques espèces de copépodes récoltés dans le Golfe de Marseille. C R Acad Sci Paris (serie D) 277:529–532

Chesney EJ (2008) Foraging behavior of bay anchovy larvae, *Anchoa mitchilli*. J Exp Mar Biol Ecol 362(2):117–124

Clemmesen C, Sanchez R, Rossi-Wongtschowski C (1997) A regional comparison of the nutritional condition of SW Atlantic anchovy larvae, *Engraulis anchoita*, based on RNA/DNA ratios. Arch Fish Mar Res 45:17–43

Conway DVP, Coombs SH, Smith C (1998) Feeding of anchovy *Engraulis encrasicolus* larvae in the northwestern Adriatic Sea in response to changing hydrobiological conditions. Mar Ecol Prog Ser 175:35–49

Cury P, Bakun A, Crawford R, Jarre A, Quinones R, Shannon L, Verheye H (2000) Small pelagics in upwelling systems: patterns of interaction and structural changes in "wasp-waist" ecosystems. ICES J Mar Sci 57(3):603

Daewel U, Peck MA, Schrum C, StJohn MA (2008a) How best to include the effects of climate-driven forcing on prey fields in larval fish individual-based models. J Plankton Res 30(1):1

Daewel UTE, Peck MA, Kuhn W, St John MA, Alekseeva I, Schrum C (2008b) Coupling ecosystem and individual-based models to simulate the influence of environmental variability on potential growth and survival of larval sprat (*Sprattus sprattus* L.) in the North Sea. Fish Oceanogr 17 (5):333–351

Davis CS, Thwaites FT, Gallager SM, Hu Q (2005) A three-axis fast-tow digital Video Plankton Recorder for rapid surveys of plankton taxa and hydrography. Limnol Oceanogr Methods 2:59–74

de Figueiredo GM, Nash RDM, Montagnes DJS (2005) The role of the generally unrecognised microprey source as food for larval fish in the Irish Sea. Mar Biol 148(2):395–404

de Figueiredo GM, Nash RDM, Montagnes DJS (2007) Do protozoa contribute significantly to the diet of larval fish in the Irish Sea? J Mar Biol Assoc UK 87(04):843–850

Fiksen Ø, Folkvord A (1999) Modelling growth and ingestion processes in herring *Clupea harengus* larvae. Mar Ecol Prog Ser 184:273–289

Fiksen Ø, Jørgensen C (2011) Model of optimal behaviour in fish larvae predicts that food availability determines survival, but not growth. Mar Ecol Prog Ser 432:207–219

Fiksen Ø, MacKenzie BR (2002) Process-based models of feeding and prey selection in larval fish. Mar Ecol Prog Ser 243:151–164

Fiksen Ø, Utne ACW, Aksnes DL, Eiane K, Helvik JV, Sundby S (1998) Modelling the influence of light, turbulence and ontogeny on ingestion rates in larval cod and herring. Fish Oceanogr 7(3–4):355–363

Galbraith PS, Browman HI, Racca RG, Skiftesvik AB, Saint-Pierre JF (2004) Effect of turbulence on the energetics of foraging in Atlantic cod *Gadus morhua* larvae. Mar Ecol Prog Ser 281:241–257

García A, Palomera I (1996) Anchovy early life history and its relation to its surrounding environment in the Western Mediterranean basin. Sci Mar 60:155–166

Grimm V, Berger U, Bastiansen F, Eliassen S, Ginot V, Giske J, Goss-Custard J, Grand T, Heinz S, Huse G (2006) A standard protocol for describing individual-based and agent-based models. Ecol Model 198(1–2):115–126

Grimm V, Berger U, DeAngelis DL, Polhill JG, Giske J, Railsback SF (2010) The ODD protocol: a review and first update. Ecol Model 221(23):2760–2768

Grosjean P, Picheral M, Warembourg C, Gorsky G (2004) Enumeration, measurement, and identification of net zooplankton samples using the ZOOSCAN digital imaging system. ICES J Mar Sci 61(4):518

Heath MR, Gallego A (1998) Bio-physical modelling of the early life stages of haddock, Melanogrammus aeglefinus, in the North Sea. Fish Oceanogr 7(2):110–125

Hermann AJ, Hinckley S, Megrey BA, Napp JM (2001) Applied and theoretical considerations for constructing spatially explicit individual-based models of marine larval fish that include multiple trophic levels. ICES J Mar Sci 58 (5):1030

Hinckley S, Hermann AJ, Mier KL, Megrey BA (2001) Importance of spawning location and timing to successful transport to nursery areas: a simulation study of Gulf of Alaska walleye pollock. ICES J Mar Sci 58(5):1042

Hinrichsen HH, Moellmann C, Voss R, Koester FW, Kornilovs G (2002) Biophysical modeling of larval Baltic cod (*Gadus morhua*) growth and survival. Can J Fish Aquat Sci 59 (12):1858–1873

Holling CS (1966) The functional response of invertebrate predators to prey density. Entomol Soc Can 48:1–86

Hunter JR (1972) Swimming and feeding behavior of larval anchovy *Engraulis mordax*. Fish Bull 70:821–834

Hunter JR (1977) Behavior and survival of northern anchovy *Engraulis mordax* larvae. CalCOFI Rep 19:138–146

Hunter JR (1980) The feeding behavior and ecology of marine fish larvae. In: Bardach JE, Magnuson JJ, May RC, Reinhart JM (eds) Fish behavior and its use in the capture and culture of fishes. ICLARM Conf. Proc. 5 Internat'l. Center for the Living Aquatic Resources Mgmt, Manila, Philippines. pp 287–330

Irigoien X, Cotano U, Boyra G, Santos M, Alvarez P, Otheguy P, Etxebeste E, Uriarte A, Ferrer L, Ibaibarriaga L (2008) From egg to juvenile in the Bay of Biscay: spatial patterns of anchovy (*Engraulis encrasicolus*) recruitment in a non-upwelling region. Fish Oceanogr 17(6):446–462

Irigoien X, Fernandes JA, Grosjean P, Denis K, Albaina A, Santos M (2009) Spring zooplankton distribution in the Bay of Biscay from 1998 to 2006 in relation with anchovy recruitment. J Plankton Res 31(1):1–17

Kiørboe T, MacKenzie B (1995) Turbulence-enhanced prey encounter rates in larval fish: effects of spatial scale, larval behaviour and size. J Plankton Res 17(12):2319–2331

Kiørboe T, Visser AW (1999) Predator and prey perception in copepods due to hydromechanical signals. Mar Ecol Prog Ser 179:81–95

Knutsen JA (1992) Feeding behaviour of North Sea turbot (*Scophthalmus maximus*) and Dover sole (*Solea solea*) larvae elicited by chemical stimuli. Mar Biol 113(4):543–548

Kolkovski S, Arieli A, Tandler A (1997) Visual and chemical cues stimulate microdiet ingestion in sea bream larvae. Aquac Int 5(6):527–536

Kristiansen T, Fiksen Ø, Folkvord A (2007) Modelling feeding, growth and habitat selection in larval cod: observations and model predictions in a macrocosm environment. Can J Fish Aquat Sci 64:136–151

Kristiansen T, Vikebø F, Sundby S, Huse G, Fiksen Ø (2008) Modeling growth of larval cod (*Gadus morhua*) in large-scale seasonal and latitudinal environmental gradients. Deep-Sea Res II 56(21–22):2001–2011

Kristiansen T, Lough RG, Werner FE, Broughton EA, Buckley LJ (2009a) Individual-based modeling of feeding ecology and prey selection of larval cod on Georges Bank. Mar Ecol Prog Ser 376:227–243

Kristiansen T, Vikebø F, Sundby S, Huse G, Fiksen Ø (2009b) Modeling growth of larval cod (*Gadus morhua*) in large-scale seasonal and latitudinal environmental gradients. Deep-Sea Res II 56(21–22):2001–2011

Kühn W, Peck MA, Hinrichsen HH, Daewel U, Moll A, Pohlmann T, Stegert C, Tamm S (2008) Defining habitats suitable for larval fish in the German Bight (southern North Sea): an IBM approach using spatially-and temporally-resolved, size-structured prey fields. J Mar Syst 74(1–2):329–342

Lasker R (1975) Field criteria for survival of anchovy larvae: the relation between inshore chlorophyll maximum layers and successful first feeding. Fish Bull 73(3):453–462

Letcher BH, Rice JA, Crowder LB, Rose KA (1996) Variability in survival of larval fish: disentangling components with a generalized individual-based model. Can J Fish Aquat Sci 53(4):787–801

Lewis DM, Bala SI (2006) Plankton predation rates in turbulence: a study of the limitations imposed on a predator with a non-spherical field of sensory perception. J Theor Biol 242(1):44–61

Lough R, Buckley L, Werner F, Quinlan J, Edwards K (2005) A general biophysical model of larval cod (*Gadus morhua*) growth applied to populations on Georges Bank. Fish Oceanogr 14(4):241–262

MacKenzie BR (2000) Turbulence, larval fish ecology and fisheries recruitment: a review of field studies. Oceanol Acta 23(4):357–376

MacKenzie BR, Kiørboe T (1995) Encounter rates and swimming behavior of pause-travel and cruise larval fish predators in calm and turbulent laboratory environments. Limnol Oceanogr: 1278–1289

MacKenzie BR, Kiørboe T (2000) Larval fish feeding and turbulence: a case for the downside. Limnol Oceanogr 45(1):1–10

MacKenzie BR, Miller TJ, Cyr S, Leggett WC (1994) Evidence for a dome-shaped relationship between turbulence and larval fish ingestion rates. Limnol Oceanogr 39(8):1790–1799

Mann J, Ott S, Pecseli HL, Trulsen J (2005) Turbulent particle flux to a perfectly absorbing surface. J Fluid Mech 534:1–21

Mann J, Ott S, Pecseli HL, Trulsen J (2006) Laboratory studies of predator–prey encounters in turbulent environments: effects of changes in orientation and field of view. J Plankton Res 28:509–522

Mariani P, MacKenzie BR, Visser AW, Botte V (2007) Individual-based simulations of larval fish feeding in turbulent environments. Mar Ecol Prog Ser 347:155

Matsushita K (1992) How do fish larvae of limited motility encounter nauplii in the sea? Bull Plankton Soc Jpn Special Volume: 251–270

Mauchline M (1998) The biology of calanoid copepods. Adv Mar Biol 33:1–710

Morote E, Olivar MP, Villate F, Uriarte I (2010) A comparison of anchovy (Engraulis encrasicolus) and sardine (Sardina pilchardus) larvae feeding in the Northwest Mediterranean: influence of prey availability and ontogeny. ICES J Mar Sci J Cons 67(5):897–908

Motos L, Uriarte A, Valencia V (1996) The spawning environment of the Bay of Biscay anchovy (*Engraulis encrasicolus* L.). Sci Mar 60:117–140

Muelbert JH, Lewis MR, Kelley DE (1994) The importance of small-scale turbulence in the feeding of herring larvae. J Plankton Res 16(8):927–944

Munk P (1992) Foraging behaviour and prey size spectra of larval herring Clupea harengus. Mar Ecol Prog Ser 80 (2):149–158

Munk P (1997) Prey size spectra and prey availability of larval and small juvenile cod. J Fish Biol 51:340–351

Munk P, Kiørboe T (1985) Feeding behaviour and swimming activity of larval herring (*Clupea harengus*) in relation to density of copepod nauplii. Mar Ecol Prog Ser 24(1):15–21

Nogueira E, Gonzalez-Nuevo G, Bode A, Varela M, Moran XAG, Valdes L (2004) Comparison of biomass and size spectra derived from optical plankton counter data and net samples: application to the assessment of mesoplankton distribution along the Northwest and North Iberian Shelf. ICES J Mar Sci 61:508–517

O'Connell CP (1981) Development of organ systems in the northern anchovy, *Engraulis mordax*, and other teleosts 1. Integr Comp Biol 21(2):429–446

Owen R, Lo N, Butler J, Theilacker G, Alvarino A, Hunter J, Watanabe Y (1989) Spawning and survival patterns of larval northern anchovy, *engraulis mordax*, in contrasting environments—a site-Intensive study. Fish Bull 87(3):673–688

Pécseli HL, Trulsen J (2007) Turbulent particle fluxes to perfectly absorbing surfaces: a numerical study. J Turbul 8(42):1–25

Pécseli HL, Trulsen JK, Fiksen Ø (2010) Predator–prey encounter rates in turbulent water: analytical models and numerical tests. Prog Oceanogr 85(3–4):171–179

Pécseli H, Trulsen J, Fiksen Ø (2012) Predator–prey encounter and capture rates for plankton in turbulent environments. Prog Oceanogr 101:14–32

Peters RH, Downing JA (1984) Empirical analysis of zooplankton filtering and feeding rates. Limnol Oceanogr 29 (4):763–784

Platt T, Denman K (1978) The structure of pelagic marine ecosystems. Rapp Pv Réun Cons Int Explor Mer 173:60–65

Pope JG, Shepherd JG, Webb J, Stebbing ARD, Mangel M (1994) Successful surf-riding on size spectra: the secret of survival in the sea. Phil Trans R Soc London B 343:41–49

Rose K, James H, Cowan J, Clark M, Houde E, Wang S (1999) An individual-based model of bay anchovy population dynamics in the mesohaline region of Chesapeake Bay. Mar Ecol Prog Ser 185:113–132

Rosenthal H, Hempel G (1970) Experimental studies in feeding and food requirements of herring larvae (*Clupea harengus* L.). In: Steele JH (ed) Marine food chains. Edinburgh, pp 344–364

Rothschild BJ, Osborn TR (1988) Small-scale turbulence and plankton contact rates. J Plankton Res 10(3):465–474

San Martin E, Harris RP, Irigoien X (2006) Latitudinal variation in plankton size spectra in the Atlantic Ocean. Deep-Sea Res II 53(14–16):1560–1572

See JH, Campbell L, Richardson TL, Pinckney JL, Shen R, Guinasso NL (2005) Combining new technologies for determination of phytoplankton community structure in the northern Gulf of Mexico. J Phycol 41(2):305–310

Seljeset O, Vollset K, Folkvord A, Geffen A (2010) The role of prey concentration and size range in the growth and survival of larval cod. Mar Biol Res 6(3):251–262

Sheldon RW, Sutcliffe WHJ, Paranjape MA (1977) Structure of pelagic food chain and relationship between plankton and fish production. J Fish Res Board Can 34(12):2344–2353

Sourisseau M, Carlotti F (2006) Spatial distribution of zooplankton size spectra on the French continental shelf of the Bay of Biscay during spring 2000 and 2001. J Geophys Res-Oceans 111:C05S09. doi:10.1029/2005jc003063, C05s09

Stephens DW, Krebs JR (1986) Foraging theory. Princeton University Press

Sundby S, Fossum P (1990) Feeding conditions of Arctonorwegian cod larvae compared with the Rothschild-Osborn theory on small-scale turbulence and plankton contact rates. J Plankton Res 12(6):1153–1162

Theilacker GH (1987) Feeding ecology and growth energetics of larval northern anchovy, *Engraulis mordax*. Fish Bull 85 (2):213–228

Theilacker GH, McMaster MF (1971) Mass culture of the rotifer *Brachionus plicatilis* and its evaluation as a food for larval anchovies. Mar Biol 10(2):183–188

Titelman J (2001) Swimming and escape behavior of copepod nauplii: implications for predator–prey interactions among copepods. Mar Ecol Prog Ser 213:203–213

Tudela S, Palomera I, Quílez G (2002) Feeding of anchovy *Engraulis encrasicolus* larvae in the north-west Mediterranean. J Mar Biol Assoc UK 82(02):349–350

Urtizberea A, Fiksen Ø, Folkvord A, Irigoien X (2008) Modelling growth of larval anchovies including diel feeding patterns, temperature and body size. J Plankton Res 30 (12):1369–1383

Utne-Palm AC (1999) The effect of prey mobility, prey contrast, turbidity and spectral composition on the reaction distance of Gobiusculus flavescens to its planktonic prey. J Fish Biol 54(6):1244–1258

Viitasalo M, Kiørboe T, Flinkman J, Pedersen L, Visser A (1998) Predation vulnerability of planktonic copepods: consequences of predator foraging strategies and prey sensory abilities. Mar Ecol Prog Ser 175:129–142

Vikebø FB, HusebØ Å, Slotte A, Stenevik EK, Lien VS (2010) Effect of hatching date, vertical distribution, and interannual variation in physical forcing on northward displacement and temperature conditions of Norwegian spring-spawning herring larvae. ICES J Mar Sci J Cons 67(9):1948

Visser AW, Fiksen Ø (2013) Optimal foraging in marine ecosystem models: selectivity, profitability and switching. Mar Ecol Prog Ser. doi:10.3354/meps10079

Walton WE, Hairston NG, Wetterer JK (1992) Growth-related constraints on diet selection by sunfish. Ecology (Durham) 73 (2):429–437

Werner F, Ian Perry R, Gregory Lough R, Naimie C (1996) Trophodynamic and advective influences on Georges Bank larval cod and haddock. Deep-Sea Res II 43(7–8):1793–1822

Zarauz L, Irigoien X, Urtizberea A, Gonzalez M (2007) Mapping plankton distribution in the Bay of Biscay during three consecutive spring surveys. Mar Ecol Prog Ser 345:27–39

Zhou M (2006) What determines the slope of a plankton biomass spectrum? J Plankton Res 28(5):437–448